# Rheological Study on High-Density Polyethylene/ Organoclay Composites

**Youhong Tang,[1] Cheng Yang,[2] Ping Gao,[1] Lin Ye,[3] Chengbi Zhao,[4] Wei Lin[4]**
[1] *Department of Chemical and Biomolecular Engineering, The Hong Kong University of Science and Technology, Clear Water Bay, Kowloon, Hong Kong, China*

[2] *Department of Mechanical Engineering, The Hong Kong University of Science and Technology, Clear Water Bay, Kowloon, Hong Kong, China*

[3] *Centre for Advanced Materials Technology, School of Aerospace, Mechanical and Mechatronic Engineering, The University of Sydney, Sydney, NSW 2006, Australia*

[4] *Centre for Advanced Marine Materials, School of Civil Engineering and Transportation, South China University of Technology, Guangzhou 510641, China*

**Maleic anhydride-grafted polyethylene (MAPE) is investigated as a compatibilizer of polyethylene/organoclay nanocomposite. With MAPE help, partial exfoliation of the organoclay occurs in the nanocomposites with the melt compounding method for organoclay loading up to 8.0 wt%. Investigation of the rheological behaviors shows that at high frequencies or shear rates, the viscosity is essentially unaffected by the presence of organoclay; however, at low frequencies or shear rates, viscoelastic behavior alters dramatically, and this is attributed to the presence of anisotropic stacks of randomly oriented organoclay sheets and the formation of network structures. The important observations are firstly the initial stress overshooting observed in steady shear. At low shear rates, stress is much greater at the initial stage than the stress at the steady state; however, it can be eliminated by preshear at low shear rates, which means that preshearing can effectively break down the network structures and align the organoclay. Second, the normalized stress at the overshoot point is a function of the critical strain unit.** POLYM. ENG. SCI., 51:133–142, 2011. © 2010 Society of Plastics Engineers

## INTRODUCTION

The influence of filler particles on the viscoelastic properties of polymer-based composite materials is of significant technological interest because of the widespread use of fillers in polymeric products. The influence of the nature and strength of polymer–filler interactions, filler–filler interactions, and the state of dispersion of the composite on the viscoelastic properties of the matrix polymer are of considerable interest for the design of filled polymer systems with enhanced physical, thermal, and mechanical properties [1, 2]. A new class of polymer nanocomposites has been developed using highly anisotropic organic modified clay dispersed in polymeric matrices [1–3]. It is instructive to study the rheology of polymer/clay hybrids for two reasons. First, rheological properties are indicative of melt processing behavior in unit operations such as injection molding. Second, as the rheological properties of particulate suspensions are sensitive to the structure, particle size, shape, and surface characteristics of the dispersed phase, rheology potentially offers a means to assess directly the state of dispersion of nanocomposites in the melt state. Further, such studies of these systems might also lead to a better understanding of the dynamics of nanoscopically confined polymers. Thus, rheology can be envisaged as a tool that is complementary to traditional methods of material characterization, such as electron microscopy, X-ray scattering, dynamic mechanical analysis, and mechanical testing. The advantages of rheology relative to these methods are that the measurements are performed in the melt state and that a battery of different rheological methods can be used to study the responses of the nanocomposite structure to both linear and nonlinear deformations.

Polyethylene is one of the most widely used polyolefin polymers. As it does not include any polar group in its backbone, it is thought that homogeneous dispersion of clay minerals in polyethylene cannot be realized. In situ polymerization of ethylene with clay is feasible, and the

*Correspondence to*: Youhong Tang; e-mail: youhongtang@gmail.com
Youhong Tang is currently at Centre for Advanced Marine Materials, School of Civil Engineering and Transportation, South China University of Technology, Guangzhou 510641, China.
DOI 10.1002/pen.21790
Published online in Wiley Online Library (wileyonlinelibrary.com).

exfoliation of the clay has been established [4, 5]. Attempts to create nonpolar polymer/clay nanocomposites by simple melt mixing were based on the introduction of a modified oligomer to mediate the polarity between the clay surface and the polymer. Typically, maleic anhydride grafted oligomers were used as compatibilizers, such as maleic anhydride-grafted high density polyethylene [6, 7], polyolefin elastomer-grafted maleic anhydride [8], and polypropylene-grafted maleic anhydride [9] In those nanocomposite system, it was pointed out that the miscibility of the maleated oligomer with matrix polymer, and maleated oligomer with clay played key roles in the properties of the composite.

In this study, we focused on the structure and melt-state viscoelastic properties of a series of nanocomposites based on high density polyethylene (HDPE) matrix and modified montmorillonite with the introduction of polyethylene-grafted maleic anhydride (MAPE) as the compatibilizer. Rheological tests of dynamic oscillatory shear, transient stress relaxation, and steady state shear were performed. All the results demonstrated the influences of the highly anisotropic nature of the organoclay on the flow properties of the nanocomposites.

## EXPERIMENTAL

### *Materials*

The montmorillonite (Closite 20A) modified by dimethyl dihydrogenated tallow ammonium ions was supplied by Southern Clay Products. Maleic anhydride-grafted polyethylene (MAPE, 0.85 wt% maleic anhydride grafted, melt index: 1.5, melting point: 120°C) was kindly supplied by Aldrich Chemical Company, Marlex HMN6060 (high density polyethylene) with a melt flow index 6.5 g/10 min (ASTM D1238, 190°C/2.16 kg) was kindly supplied by Philips Petroleum International.

### *Preparation of Composites*

The as-received MAPE, HMN6060, and organoclay were dried at 105°C in an oven for at least 12 h before use. A Hakke9000 twin-screw extruder was used with four heating zones with temperatures of 130°C, 160°C, 190°C, and 160°C, respectively, and the rotation speed was 5.0 rpm and 40.0 rpm separately for two successive extrusions. Several types of nanocomposite with different weight ratios of organoclay and the same weight ratio of MAPE were prepared, and several types of composite with different weight ratios of organoclay and without MAPE were prepared for comparison. Table 1 gives the details of the composites.

### *Characterization Methods*

Wide angle X-ray diffraction (WAXD) was conducted on a Philips powder X-ray diffraction system Model PW 1830 with Cu kα radiation of wavelength 1.54 Å. Transmission electron microscope (TEM) samples were prepared by cryogen-ultramicrotomed with glass knives on a Leica ultracut microtome under a temperature of −100°C to yield sections with a nominal thickness of 100 nm. TEM images were obtained at 120 KV with a Philips CM20 electron microscope.

TABLE 1. Composition of blends.

| | HMN6060 (wt %) | MAPE (wt %) | Organoclay (wt %) |
|---|---|---|---|
| PM | 65 | 35 | 0 |
| PMC1 | 64 | 35 | 1 |
| PMC3 | 62 | 35 | 3 |
| PMC5 | 60 | 35 | 5 |
| PMC8 | 57 | 35 | 8 |
| PC3 | 97 | 0 | 3 |
| PC5 | 95 | 0 | 5 |

Controlled strain measurements were carried out to characterize the rheological behaviors of these composites using the advanced rheometric expansion system (ARES). Twenty-five millimeter parallel plate fixtures were used for all tests reported here. All measurements were performed at 190°C with a 2000 g cm transducer within the resolution limit of 2 g cm and a 200 g cm transducer within the resolution limit of 0.2 g cm. Before each experiment, the system was preheated and equilibrated at the test temperature for at least 30 min. Viscoelasticity responses of the materials were also characterized by employing a capillary rheometer, Göttfert Rheograph 2003A. Two types of capillary dies were used. One type had a constant 1.0 mm diameter, with length to diameter ratios ($L/D$) equal to 1, 15, and 30 respectively, and the other had a constant $L/D$ ratio of 30 but different diameters. The die entrance angle was 180°. All the experiments were performed at 190°C and all the materials had been dried in an oven at 105°C for 12 h before testing.

## RESULTS AND DISCUSSION

### *Morphology of Composites*

WAXD is a rather simple and widely used technique for characterization of clay dispersion. The organoclay and organoclay-related composite X-ray patterns are presented in Fig. 1. As is evident in Fig. 1, the characteristic plane (001) diffraction peak of the organoclay is around $2\theta = 3.75°$ ($d$-spacing: 2.35 nm) and the peak positions of 3.0 wt% clay/HMN6060 (PC3) and 5.0 wt% clay/HMN6060 (PC5) composites shift only marginally to $2\theta = 3.0°$ ($d$-spacing: 2.94 nm). With the introduction of MAPE, the (001) peak disappears in 1.0 wt% clay/35.0 wt% MAPE/HMN6060 (PMC1), or exhibits a relatively insignificant peak or shoulder with a gradual increase in the diffraction strength toward low angles in 3.0 wt% clay/35.0 wt% MAPE/HMN6060 (PMC3), 5.0 wt% clay/35.0 wt% MAPE/HMN6060 (PMC5), and 8.0 wt% clay/35.0 wt% MAPE/HMN6060 (PMC8). These results clearly indicate the exfoliated or intercalated capabilities of the organoclay with assistance of the compatibilizer

 DOI 10.1002/pen

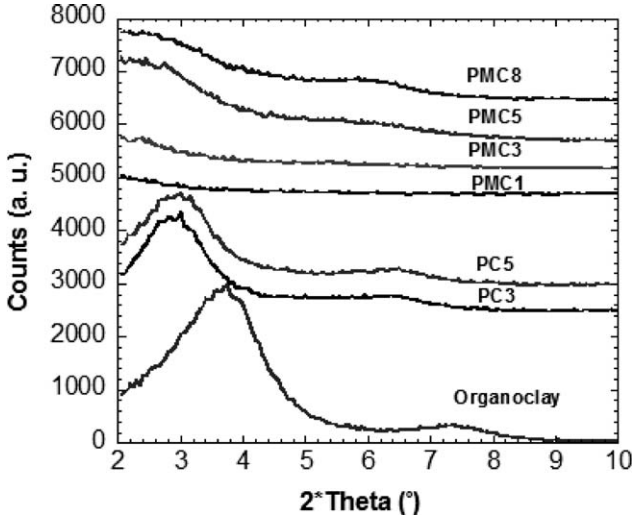


FIG. 1. WAXD patterns of organoclay, polyethylene/organoclay composites (PC3 and PC5) and polyethylene/MAPE/organoclay composites (PMC1, PMC3, PMC5, and PMC8).

(MAPE). TEM images of the PC5 and PMC5 composites are shown in Fig. 2(a) and (b). In the PC5, the organoclay stacks together and the peak in the WAXD pattern is attributed to these unopened layers. In the PMC5, both stacked (intercalated) and isolated (exfoliated) clay layers are observed. The existence of the small peak or shoulder in the WAXD patterns of this sample is attributed to the nonexfoliated layers.

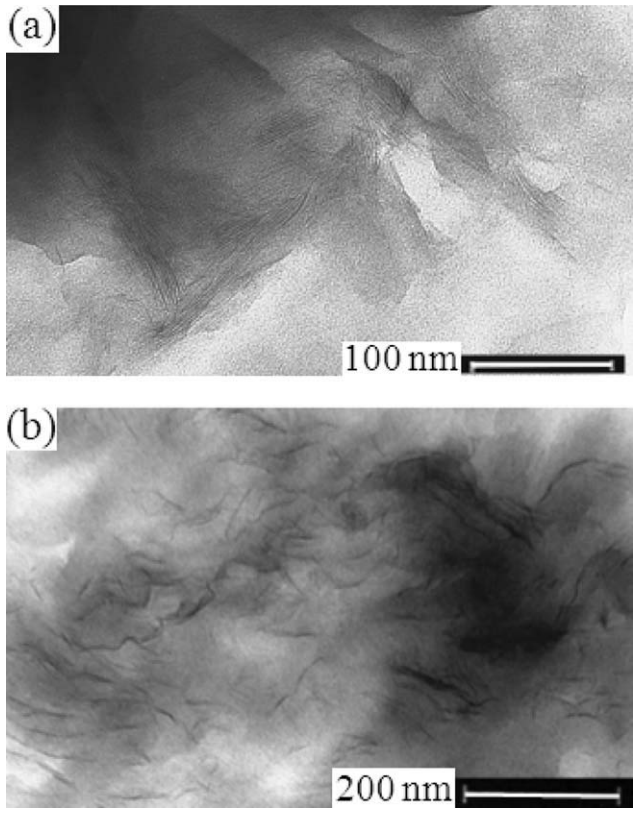


FIG. 2. TEM images of (a) PC5 and (b) PMC5.

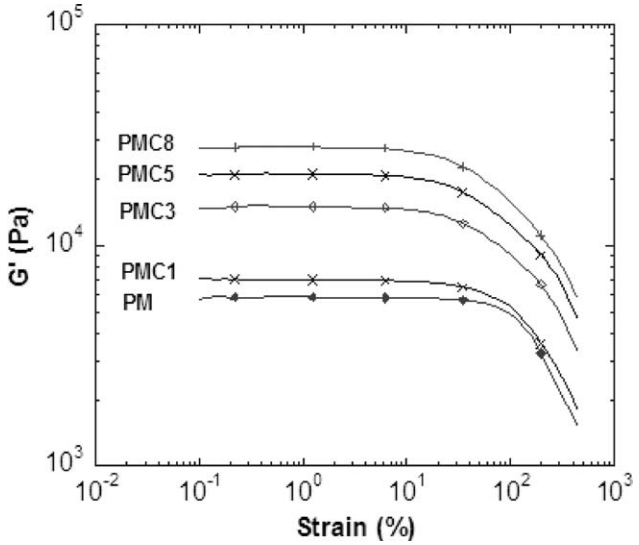


FIG. 3. Dynamic strain sweep of nanocomposites with different organoclay loading.

*Rheological Properties*

**Dynamic Viscoelasticity Behaviors.** The transition from linear to nonlinear viscoelastic behaviors in the unfilled polymer and its nanocomposites, as manifested in dynamic strain sweep experiments with storage modulus, is shown in Fig. 3. The storage modulus exhibits the expected shear-thinning behavior, with the critical strain amplitude for the transition decreasing with increased organoclay loading. Further, the strain amplitude dependence of the storage modulus in the shear-thinning regime increases with increasing organoclay content.

The organoclay is dispersed in the polymeric matrix as both a few individual layers and stacks of layers (as observed in Fig. 2b), which are randomly organized under the quiescent condition. With the application of increasing amplitude of oscillatory shear, the layers or stacks gradually orient themselves and align parallel to the flow direction. This orientation can be considered analogous to that observed in liquid crystals and block copolymers, with no effective change in the interlayer spacing and with no ironing out of intergranular defects. Further, it is expected that in the quiescent state, with increased clay loading, a larger fraction of the stacks would be hydro-dynamically hindered, resulting in the filler–filler interaction becoming increasingly important and in fact dominating the long-term viscoelasticity of the nanocomposites. Additionally, with increased clay loading, the ease with which the clay structure can be altered by flow is considerably enhanced, primarily because of increasing filler–filler interactions. Based on the above, it is not surprising that the threshold strain amplitude for the onset of shear-thinning decreases with increasing clay loading and the strain amplitude dependence of shear thinning is enhanced for the nanocomposites with higher clay loadings.

The dependence of dynamic viscoelastic behavior on the organoclay concentration was investigated and the

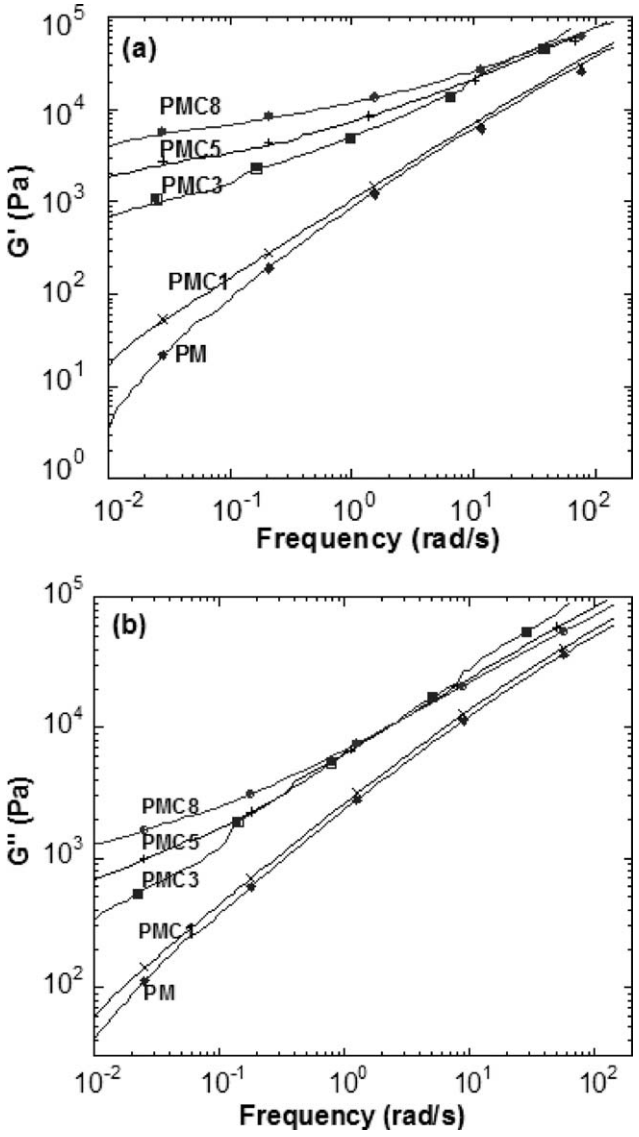


FIG. 4. (a) Storage and (b) loss moduli changing with frequencies for different organoclay loading nanocomposites.

master curves for the control matrix and the different nanocomposites are shown in Fig. 4. At all frequencies, both storage modulus and loss modulus for the nanocomposites increase monotonically with increased organoclay loading. Viscoelastic behavior at high frequencies is unaffected by the addition of organoclay. However, at lower frequencies, both $G'$ and $G''$ exhibit diminished frequency dependence, with the frequency dependence becoming weaker with increasing organoclay content. For the PMC3, PMC5, and PMC8 nanocomposites, in the low frequency regions, storage modules are nearly independent of frequency. The observation suggests the possibility of pseudo-solid-like behavior for time scales at least of the order of $10^2$–$10^3$ s.

The low-frequency viscoelastic response can be explained in terms of physical jamming of the dispersed organoclays due to their highly anisotropic nature. The frequency dependence of the low frequency $G'$ and $G''$ is similar to that observed in PEO/organoclay nanocomposites [10]. Because of the highly anisotropic nature of the organoclay and simple geometric constraints, the layers would exhibit local correlations. These local correlations cause the presence of domains and, similar to studies of liquid crystalline and ordered block copolymer systems [11–14], the presence of these domains causes the enhanced low-frequency modulus and the related low power-law dependence.

Figure 5 presented is $\tan\delta = G''/G'$ versus frequencies for nanocomposites. For $\tan\delta = G''/G' > 1$ ($G'' > G'$), we expect liquid-like behavior; for $\tan\delta = G''/G' < 1$ ($G' > G''$) and $G'$ is nearly independent of frequency, we expect solid-like behavior. The melt behaviors of the PM and PMC1 are liquid-like in the measured frequency regimes. PMC3, PMC5, and PMC8 display solid-like behaviors at low frequencies, whereas liquid-like behaviors are found at high frequencies. The transition frequencies are about 0.2 and 2.0 rad/s for PMC3 and PMC5, respectively, as indicated by $\tan\delta = 1$, and no transition frequency is found in the given frequency regions for PMC8. The transition frequency position shifts toward a higher frequency with increased organoclay content and the solid-like behaviors of the PMC nanocomposites become stronger and even dominant across the whole frequency range.

The formation of a three-dimensional network in partially exfoliated clay in a polymeric matrix is similar to the phenomenon in physical gels such as plasticized PVCs, in which a three-dimensional network is formed from flexible chains through physical phase transformation [15]. The critical change from the liquid state to the solid state is known as the sol-gel transition (gel point) at which rheologically the zero-viscosity and relaxation time of the system diverges. It is important to know how to determine this gel point. Traditionally, many researchers use the crossover of $G''$ and $G'$ as an indicator of the gel

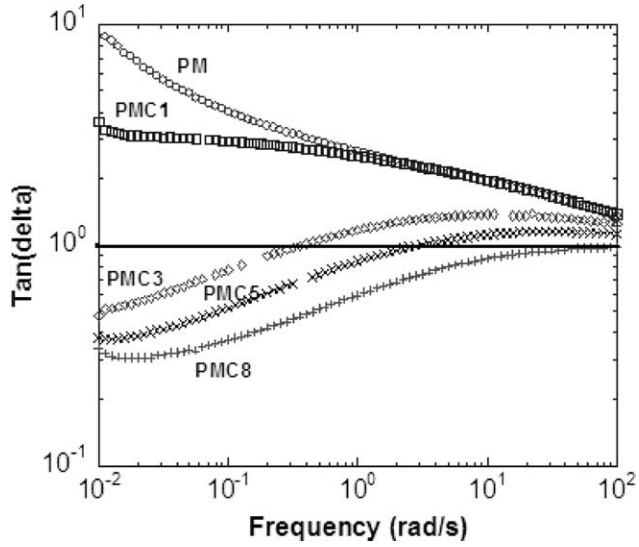


FIG. 5. tan $\delta$ changing with frequencies for different organoclay loading nanocomposites.


DOI 10.1002/pen

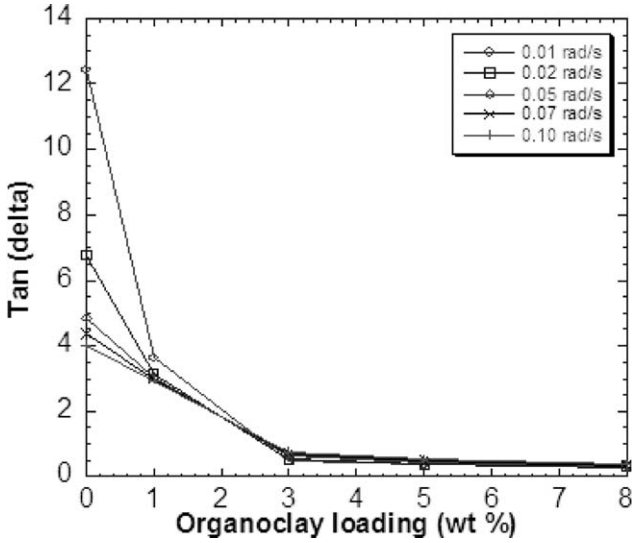


FIG. 6. The gelatin point in the PMC nanocomposites.

point. This method is simple and convenient, but not valid in general. Winter and co-workers [16] first experimentally found a scaling law and later generalized it to $G'(\omega) \sim G''(\omega) \sim \omega^n$ for $0 < n < 1$ or $G''(\omega)/G'(\omega) = \tan \delta = \tan(n\pi/2)$ for all gelling systems [17, 18]. Here, we use the "gelatin point" conception in our nanocomposites and determine the critical organoclay concentration in them. The method is known as the frequency-independence of tan $\delta$. The gel point is determined from a multifrequency plot of tan $\delta$ versus clay concentration, which governs liquid-solid transition. The "gel point" has been well determined using this method. All curves in Fig. 6 pass through the same point at a certain organoclay loading ($\sim$2.4 wt %), which is defined as the critical concentration of organoclay in the nanocomposite. The critical exponent n is simply calculated from the gel point using the relation $G''(\omega)/G'(\omega) = \tan \delta = \tan(n\pi/2)$, that is, $n = 0.796$ in our system. In general, a lower value of $n$ implies the formation of more highly elastic properties [15].

**Stress Relaxation.** To confirm the unusual viscoelastic behavior observed at low frequencies in the dynamic measurements for the organoclay nanocomposites, stress relaxation measurements were carried out and the results are shown in Fig. 7. For any fixed time after the imposition of strain, the modules increase with increasing organoclay loading, in a manner similar to that observed in the dynamic viscoelastic measurements. Further, at short time spans (for $t < 0.05$ s), the stress relaxation behavior is qualitatively similar for all the composites and the unfilled matrix. With long time spans, however, the unfilled matrix PM and the composite PMC1 relax like liquid, whereas the others behave in a solid-like manner for as long as $\sim$500 s. On the basis of both dynamic oscillatory shear and stress relaxation modulus, it is clear that the addition of organoclays has a profound influence on the long time span relaxation of the nanocomposites. With increased clay loading, the liquid-like relaxation observed for the unfilled polymer gradually changes to solid-like behavior in the nanocomposites with organoclay loading in excess of 3.0 wt%.

The nonlinear stress relaxation measurements at a strain amplitude of 700.0% with different organoclay contents are given in Fig. 7b. This shows similar shapes to the stress relaxation in the linear region as in Fig. 7a, but the corresponding $G(t)$ is smaller than that in the linear stress relaxation test. The most likely reason is that although the large amplitude and nonlinear stress suddenly imposed on the melt nanocomposites can cause stacks of clay or individual clay layers to align parallel to the imposed strain direction, after the cessation of strain the stacks or individual layers cannot fully relax, which results in a corresponding shear stress relaxation modulus lower than that in linear stress relaxation experiment.

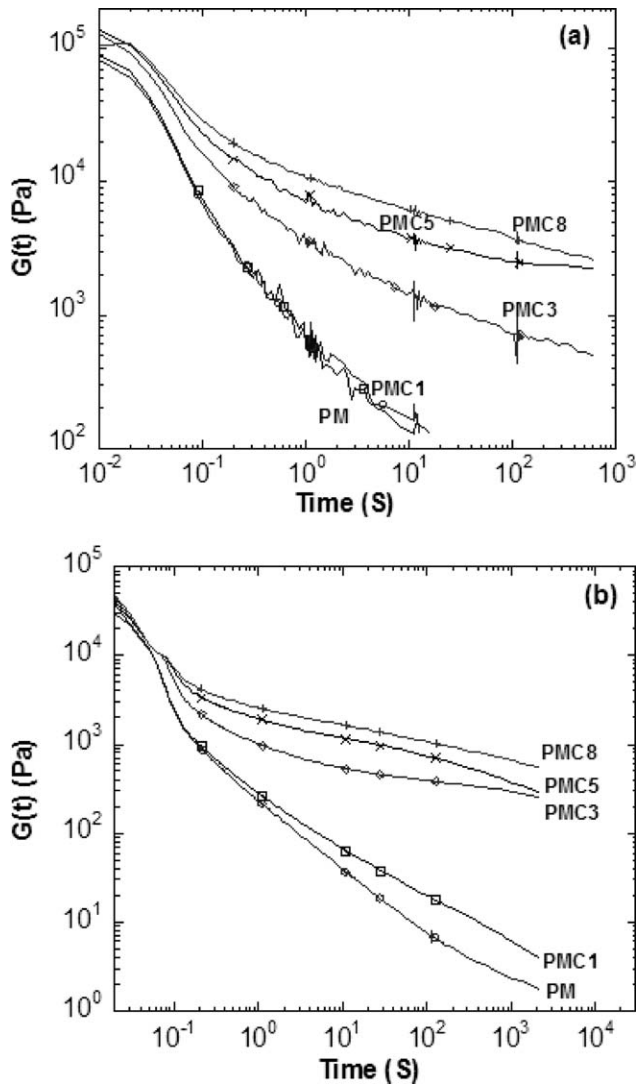


FIG. 7. Stress relaxation in (a) linear and (b) nonlinear (strain = 700.0%) regions for nanocomposites with different organoclay loading.

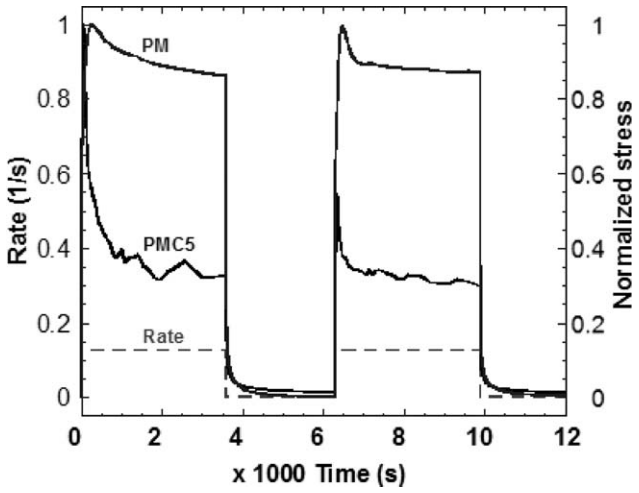


FIG. 8. Typical steady shear graphs of PM composite and PMC5 nanocomposite.

**Preshear Effects.** Application of a steady shear rate leading to a shear-aligned sample is a more effective method to align the structure of the samples. This measurement was carried out on the PMC5 nanocomposites and the apparent shear viscosity showed a decrease with continued shearing and finally reached a plateau value. With the exception of the first few minutes of shear for the PMC5 composite, the stress decreased monotonically. In the first few minutes of shearing, the stress reached a maximum before monotonically decreasing, as shown in Fig. 8. The dynamic frequency sweep after steady state shearing is shown in Fig. 9. First, both the storage and loss modulus for the presheared sample were considerably lower than those for the initially unpresheared sample. Second, the frequency dependence of both $G'$ and $G''$ was much stronger for the presheared samples, indicating after preshear, the solid-like behavior that existed in the original sample was destroyed or weakened and not easy to rebuild.

**Steady Shear Behavior.** The transient response to nonlinear deformation is perhaps a more effective test, as structural evolution and relaxation can be quantified. Step rate tests were performed and the following deformation history was applied to the sample: First, the sample was sheared for 3600 s at shear rate 0.1259 1/s to reach a steady state. Next, the flow was stopped and the sample was held quiescent for a time that varied according to the experiment. Finally, the sample was subjected to the same shear rate again for 3600 s. The shear stress was monitored during those periods. Figure 8 shows the typical stress response with deformation. The PM matrix shows a slight increase in stress before a monotonic decrease, and after a period of relaxation, when the same shear rate is applied to the composites again, the stress curve again shows the same overshoot phenomenon. Figure 8 also shows the response of the PMC5 nanocomposites displaying the deformation with time. The stress response displays a similar overshoot, the magnitude being greater than that of PM. After a period of relaxation, the stress overshoot still exists but with a relatively lower magnitude. Note that the stress overshoot observed in the transient rheological experiments is attributed to the organoclays and the interactions of organoclay with the polymer, not to the viscoelasticity of the polymeric matrix itself. A number of researchers have studied the disorientation after large deformation "aligning" the organoclays. The mechanism for this partial recovery has been suggested to be the result of a quiescent non-Brownian structural origin [19–21] or to be Brownian [22]. Using in situ X-ray scattering, Lee and co-workers [19] suggested that compatibilized syndiotactic polypropylene nanocomposite initially disoriented rapidly (much faster than Brownian motion) and then remained in a constant orientation state for a time period of $\sim$1500 s. They argued that the rapid initial decrease in orientation was a result of the coupling of the polymer chains to the clays and was not a result of attraction between clay layers. Ren and co-workers [20] reported that the disorientation process exhibited signatures of aging also observed in soft-colloidal glasses, which was shown to be independent of temperature, nanoparticle size and chemical details, viscoelasticity and molecular weight of the polymer matrix.

The stress response upon start-up of steady shear was measured at a number of shear rates to further investigate the time evolution of the stress. The following deformation history was applied to the sample: First, the shear rate 0.1259 1/s was applied to the sample for 3600 s to reach a steady state plateau. Next, a specified relaxation time (5400 s) was allowed, by which the organoclay layers would have achieved their maximum recovery towards the original state. After those two steps, the samples had the same rheological history. Then, different shear rates were applied to the sample for 3600 s. Finally, the sample was held quiescent again. Results for the

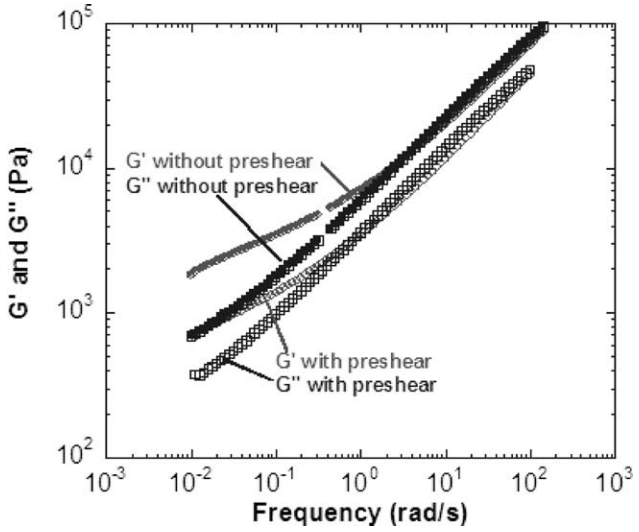


FIG. 9. Dynamic frequency sweep before and after preshear for PMC5 nanocomposite.

 DOI 10.1002/pen

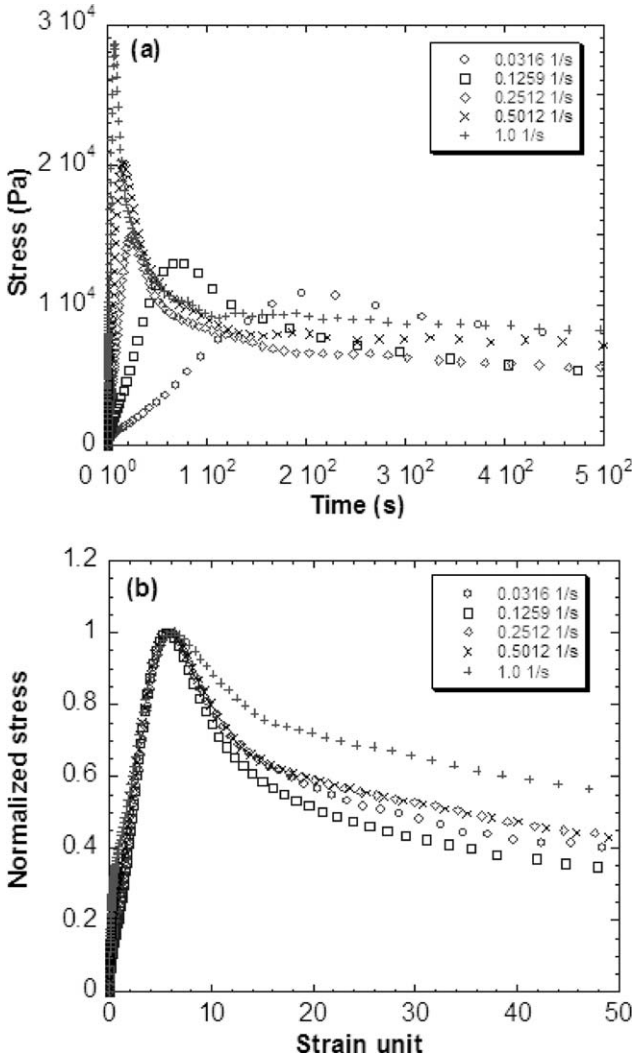


FIG. 10. (a) Stresses and (b) normalized stresses change with different shear rates histories in step rate test for PMC5 nanocomposite.

PMC5 nanocomposite are plotted in Fig. 10a. Shear rates between 0.03 and 1.0 1/s are probed. The magnitude of stress overshoot of flow is a strong function of shear rate and shear time. The dependence can be better understood if the stress response is plotted with the strain unit. The resulting curves are plotted in Fig. 10b with normalized stress. Figure 10b supports the conclusion that the stress at the start-up of steady shear scales with the applied strain for this nanocomposite. Strain scaling of stress is characteristic of materials that possess no characteristic time scale. Examples of such materials include textured liquid crystalline polymer solutions and non-Brownian suspensions of rods and disks.

In the rheological characterization of the nanocomposite, the steady shear response of the clay based polymer nanocomposite provides useful information on the processability of the material. The steady shear viscosity as a function of shear rate is shown in Figs. 11 and 12.

Figure 11 shows the shear viscosity measured in parallel plates geometry by ARES in step rate testing with

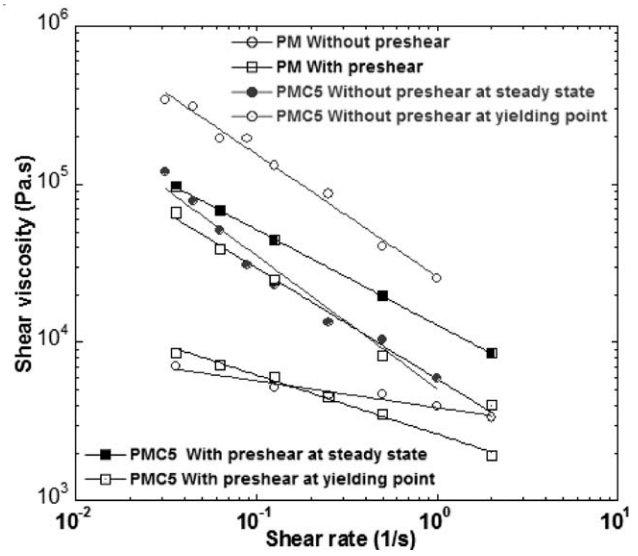


FIG. 11. Shear viscosities for PM at steady state and PMC5 at steady state and yielding point with and without preshear. (Points are experimental data; lines are power-law constitutive equation fitting curves).

shear rates varying between 0.03 1/s and 2.0 1/s. The shear viscosities of the PM with and without preshear at steady state and the PMC5 nanocomposites with and without preshear at steady state and also at yielding points were measured with different shear rates. The viscosities in the steady states of the nanocomposites are much higher than those of the PM matrix. This enhancement arises from the interaction and dispersion of organoclay in the polymeric matrix. With increasing shear rate the difference between the shear viscosities decreases. In other words, at low shear rates, the addition of very small amounts of organoclay results in a significant enhancement in the shear viscosity. However, at relative high shear rates, the shear viscosity and shear thinning behav-

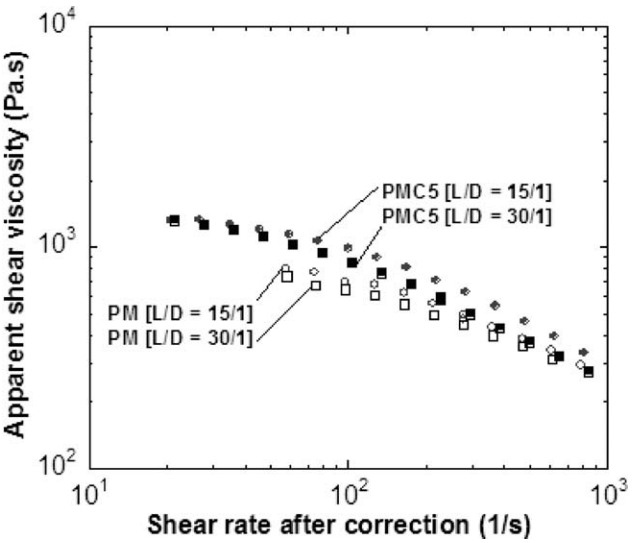


FIG. 12. Data of capillary rheometer experiment of PM and PMC5 nanocomposite with different L/D ratio in 190°C after corrections.

TABLE 2. Parameters in power law model for PM and PMC5 nanocomposites.

| | | PM | | PMC5 | |
|---|---|---|---|---|---|
| | | $k$ | $n$ | $k$ | $n$ |
| With preshear | Steady state | 2628.1 | 0.626 | 12888 | 0.397 |
| | Overshoot point | – | – | 5871.9 | 0.298 |
| Without preshear | Steady state | 3872.2 | 0.831 | 5102.8 | 0.159 |
| | Overshoot point | – | – | 26025 | 0.227 |

ior of the nanocomposites are comparable with those of the polymeric matrix as a result of the preferential orientation of clay layers parallel to the flow direction.

As illustrated in Fig. 11, the flow curves of the PM and PMC5 nanocomposites with and without preshear can be fitted by the power law model. The viscosity decreases linearly with increasing shear rates on log-log plots. The parameters in the power law model are listed in Table 2. We find that $n$ decreases after preshearing for the PM composite but increases for the PMC5 nanocomposite both at steady and yielding conditions. After sufficient steady state shear, the chains in the PM composite are partially aligned parallel to the flow field, causing the PM to perform more like solid, so $n$ decreases. However, the network structure found in the PMC5 nanocomposite is destroyed and the partial orientation formed by steady state shear causes the PMC5 nanocomposite to perform more like liquid, so $n$ increases after preshear. The magnitudes of shear viscosity at yielding points before and after preshear are dramatically different, owing to the orientation of intercalated chains and ordered clay layers aligned parallel to the flow direction, but the change in magnitude of $n$ is not significant, the probable reason being that the degree of organoclay orientation in the polymeric matrix induced by the shear flow is almost constant even after preshearing and relaxation. Therefore, the degree of clay layer orientation cannot change greatly, and it is almost the same as the sample without preshearing.

In highly elastic fluid and polymer melts, it is very difficult to measure the steady shear viscosity at high shear rates. A capillary rheometer is used to characterize rheological properties at high shear rates; this is important because it allows us to determine the shear rate dependence if the viscosity at shear rates significantly higher than those permitted for cone-plate and parallel plate geometries. Figure 12 gives the plot of apparent shear viscosities versus apparent shear rates. Rabinowitsch [23] and Bagley [24] correction are used to correct the apparent shear rates and shear stresses at wall (or entrance pressure). After these corrections, the master-curves of the PM and PMC5 nanocomposites with different $L/D$ ratios ($L/D = 15$ and 30) coincide with each other. Figure 12 also shows results, which are consistent with the dynamic viscoelastic experiment and stress relaxation experiment; that is, in the high shear rate regimes (high frequencies or short times), the nanocomposites are essentially unaffected by the addition of organoclays but in the low shear rates regimes (low frequencies or long times), the viscoelastic response for the nanocomposites displays a phenomenon of significant dependence on organoclay content.

Shear viscosity can be estimated from the Cox-Merz relation [25]. Figure 13 shows that the complex viscosity and shear viscosity of the PMC5 nanocomposite obtained from the oscillatory experiments and steady shear experiment as a function of frequency and shear rate. Both complex viscosity and apparent shear viscosity decrease with increasing frequencies and apparent shear rate, but they do not fit together. This deviation is possibly attributable to the orientation of the clay layers. Note that oscillatory shear, when applied in the linear viscoelastic region, may be able to promote the shear thinning capability of the materials. In contrast, steady shear can effectively rearrange the molecular packing of the materials along the shear direction when sufficient strain is applied. Thus, the Cox-Merz relation for the PMC5 nanocomposites is invalid.

### *Modeling of Data by Constitutive Equations*

We attempt to model the step rate test data using the Wagner equation model [26]. On the basis of general elastic theory, which is independent of molecular structure, this constitutive equation has been shown to work well for the cases of mesostructured block copolymer micelles- and silica particle-loaded polymer composites [27]. Following the Wagner equation model, the shear stress in simple shear is given as

$$\sigma_{12}(t) = -\int_{-\infty}^{t} M(t-t')\gamma(t,t')\Phi(\gamma)dt' \qquad (1)$$

where $M(t-t')$ is the memory function, $\Phi(\gamma)$ is the damping function.

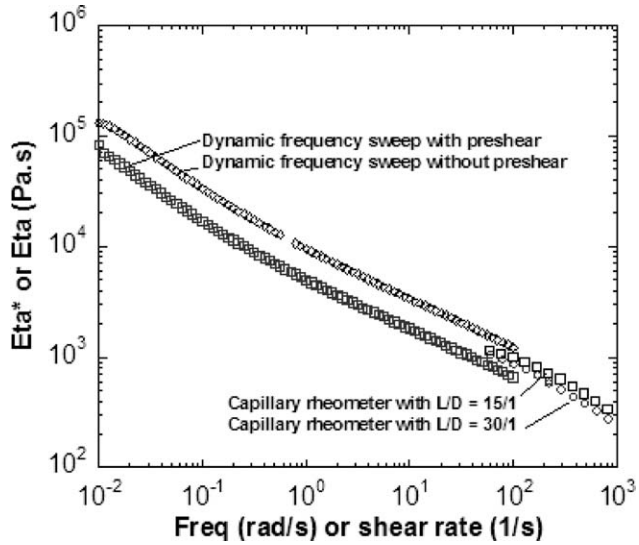


FIG. 13. Apparent shear viscosity and complex viscosity as the function of apparent shear rate and frequency for PMC5 nanocomposite.

In the Wagner equation, $\Phi(\gamma) = \exp(-k|\gamma(t, t')|)$ and $k$ is the damping coefficient in the damping function, which can be calculated by the following equation:

$$k = -\frac{1}{\gamma}\ln\frac{G(t,\gamma)}{G(t)} \tag{2}$$

where $G(t, \gamma)$ and $G(t)$ are the stress relaxation moduli in the nonlinear and linear regions, respectively.

Here, we use the Wagner equation model to predict the start-up of steady flow, the shear rate independence of the normalized steady state viscosity, and the stress relaxation after cessation of steady state shear, and we compare them with the experimental data for the nanocomposites reported here.

Stress Growth Versus Time (First Stage)

$$\sigma(t) = \sum_{i=1}^{N}\frac{g_i\dot{\gamma}_0}{1+\lambda_i k\dot{\gamma}_0}t\cdot\exp(-\alpha t) + \sum_{i=1}^{N}\frac{g_i\dot{\gamma}_0\lambda_i}{(1+\lambda_i k\dot{\gamma}_0)^2}[1-\exp(-\alpha t)] \tag{3}$$

where $\alpha = \frac{k\dot{\gamma}_0\lambda_i+1}{\lambda_i}$

Steady State Stress Versus Shear Rate (Second Stage)

$$\sigma(t) = \sum_{i=1}^{N}\frac{g_i\dot{\gamma}_0\lambda_i}{(1+\lambda_i k\dot{\gamma}_0)^2} \tag{4}$$

Stress Relaxation after Shear Rate (Third Stage)

$$\sigma(t) = \sum_{i=1}^{N}\frac{g_i\dot{\gamma}_0}{\lambda_i\alpha}(t\cdot\exp(-\alpha t) + \frac{1}{\alpha}\exp(-\alpha t)) \tag{5}$$

where $\alpha = \frac{k\dot{\gamma}_0\lambda_i+1}{\lambda_i}$

The Wagner equation model, using linear and nonlinear stress relaxation modulus to describe the nonlinear damping function and combining with frequency sweep data, is clearly inadequate to predict the intermediate shear rate viscosity data for nanocomposites (especially the overshoot phenomenon) as shown in Fig. 14a. During the steady shear rate tests, the sample slowly evolved to a final mesoscale oriented structure with normalized steady shear viscosity independent of the shear rates and accurately predicted by Wagner equation model, which means that the factorability of strain and time in the model is acceptable in this condition. During stress relaxation tests, Fig. 14b shows that the sample evolves to recover in the quiescent condition. The relaxation trend can be predicted but with longer relaxation time. The inability of the Wagner equation model to predict the intermediate shear rate data (start-up and relaxation of steady flow) suggests that the nanocomposites undergo changes in their mesoscale structure at those shear rates that lead to rheological behavior not encountered in the determination of the damping functions via the step-strain measurements.

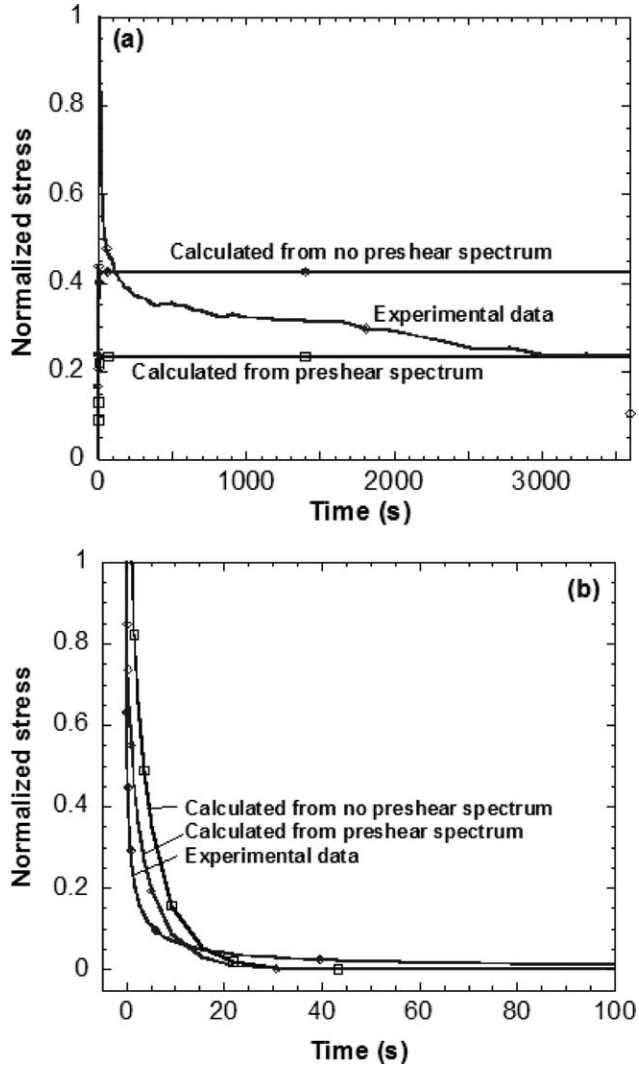


FIG. 14. PMC5 step rate test of shear rate 1.0 1/s calculated from Wagner equation and from experimental data at (a) stress growth and steady states and (b) stress relaxation state.

## CONCLUSIONS

Significant changes in viscoelastic properties depending on the mesoscopic structure and strength of polymer-organoclay interactions were observed in rheological testing. Non-Newtonian viscosity behavior was observed at all organoclay loadings, and the low-frequency storage modulus developed a plateau. Storage and loss moduli increased monotonically with increased organoclay loading. Viscoelastic behaviors at high frequencies were unaffected by the addition of organoclay. However, at low frequency, both storage and loss moduli exhibited diminished frequency dependence, with the frequency dependence becoming weaker with increased organoclay loading. Results from the capillary rheometer coincided quite well with those from the dynamic frequency sweep

and stress relaxation tests in the linear and nonlinear regions. The step rate tests in the PMC5 nanocomposite showed dramatic stress overshoot. This was a strain dependent phenomenon, which was easily erased when the deformation reached a certain value. The normalized critical stress was a function of the critical strain unit. The Cox-Merz rule could combine the results from the dynamic frequency sweep with and without preshearing and the capillary rheometer data after correction.

## REFERENCES


1. P. Cassagnau, *Polymer*, **49**, 2183 (2008).
2. E.P. Giannelis, *Adv. Mater*., **8**, 29 (1996).
3. E.P. Giannelis, R. Krishnamoorti, and E. Manias, *Adv. Polym. Sci*., **138**, 107 (1999).
4. Y.H. Jin, H.J. Park, S.S. Im, S.Y. Kwak, and S. Kwak, *Macromol. Rapid Commun*., **23**, 135 (2002).
5. S. Ray, G. Galgali, A Lele, and S. Sivaram, *J. Polym. Sci. Part A: Polym. Chem*., **43**, 304 (2005).
6. M.W. Spencer, L.L. Cui, Y. Yoo, and D.R. Paul, *Polymer*, **51**, 1056 (2010).
7. J. Cao, K. Wang, H. Yang, F. Chen, Q. Zhang, and Q. Fu, *J. Polym. Sci. Part B: Polym. Phys*., **48**, 302 (2010).
8. S.M. Lai, W.C. Chen, and X.S. Zhu, *Composite: Part A*, **40**, 754 (2009).
9. D. Marchant and K. Jayaraman, *Ind. Eng. Chem. Res*., **41**, 6402 (2002).
10. Y.H. Hyun, S.T. Lim, H.J. Choi, and M.S. Jhon, *Macromolecules*, **34**, 8084 (2001).
11. G.H. Fredrickson and F.S. Bates, *Annu. Rev. Mater. Sci*., **26**, 501 (1996).
12. R.G. Larson, K.I. Winey, S.S. Patel, H. Watanabe, and R. Bruinsma, *Rheol. Acta*., **32**, 245 (1993).
13. R.H. Colby, *Curr. Opin. Colloid Interface Sci*., **1**, 454 (1996).
14. M.B. Kossuth, D.C. Morse, and F.S. Bates, *J. Rheol*., **43**, 167 (1999).
15. L. Li and Y. Aoki, *Macromolecues*, **30**, 7835 (1997).
16. F. Chambon and H.H. Winter, *Polym. Bull*., **13**, 499 (1985).
17. H.H. Winter and F. Chambon, *J. Rheol*., **30**, 367 (1986).
18. F. Chambon and H.H. Winter, *J. Rheol*., **31**, 683 (1987).
19. A. Lele, M. Mackley, G. Galgali, and C. Ramesh, *J. Rheol*., **46**, 1091 (2002).
20. J.X. Ren, B.F. Casanueva, C.A. Mitchell, and R. Krishnamoorti, *Macromolecules*, **36**, 4188 (2003).
21. M.J. Solomon, A.S. Almusallam, K.F. Seefeldt, A. Somwangthanaroj, and P. Varadan, *Macromolecules*, **34**, 1864 (2001).
22. R.G. Larson, *The Structure and Rheology of Complex Fluid*, Oxford University Press, New York (1999).
23. B. Rabinowitsch, *J. Phys. Chem. A*, **145**, 1 (1929).
24. E.B. Bagley, *Trans. Soc. Rheol*., **5**, 355 (1961).
25. W.P. Cox and E.H. Merz, *J. Polym. Sci*., **28**, 619 (1958).
26. M.H. Wagner, *Rheol. Acta*., **15**, 136 (1976).
27. M.R. Mackley, R.T.J. Marsheall, J.B.A.F. Smeulders, and D.F. Zhao, *Chem. Eng. Sci*., **49**, 2551 (1994).


 DOI 10.1002/pen